

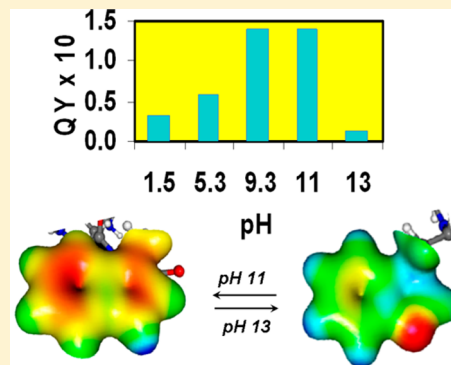
The Broken Ring: Reduced Aromaticity in Lys-Trp Cations and High pH Tautomer Correlates with Lower Quantum Yield and Shorter Lifetimes

Azaria Solomon Eisenberg* and Laura J. Juszczak*

Department of Chemistry, Brooklyn College of The City University of New York, 2900 Bedford Ave., Brooklyn, NY 11210, United States

Supporting Information

ABSTRACT: Several nonradiative processes compete with tryptophan fluorescence emission. The difficulty in spectral interpretation lies in associating specific molecular environmental features with these processes and thereby utilizing the fluorescence spectral data to identify the local environment of tryptophan. Here, spectroscopic and molecular modeling study of Lys-Trp dipeptide charged species shows that backbone-ring interactions are undistinguished. Instead, quantum mechanical ground state isosurfaces reveal variations in indole π electron distribution and density that parallel charge (as a function of pK_1 , pK_2 , and pK_R) on the backbone and residues. A pattern of aromaticity-associated quantum yield and fluorescence lifetime changes emerges. Where quantum yield is high, isosurfaces have a charge distribution similar to the highest occupied molecular orbital (HOMO) of indole, which is the dominant fluorescent ground state of the 1L_a transition dipole moment. Where quantum yield is low, isosurface charge distribution over the ring is uneven, diminished, and even found off ring. At pH 13, the indole amine is deprotonated, and Lys-Trp quantum yield is extremely low due to tautomer structure that concentrates charge on the indole amine; the isosurface charge distribution bears scant resemblance to the indole HOMO. Such greatly diminished fluorescence has been observed for proteins where the indole nitrogen is hydrogen bonded, lending credence to the association of aromaticity changes with diminished quantum yield in proteins as well. Thus tryptophan ground state isosurfaces are an indicator of indole aromaticity, signaling the partition of excitation energy between radiative and nonradiative processes.



INTRODUCTION

Understanding the factors responsible for Trp fluorescence changes is critical to interpretation of biologically relevant, solvent-phase protein structure. The basis for the observed thirty-fold variation^{1,2} in tryptophan (Trp) fluorescence emission intensity (quantum yield) in proteins has been under study for the last 40 years.^{3–14}

Within the past 20 years, the role of charge transfer has gained increasing importance in explaining fluorescence changes in intensity, lifetime, and wavelength and is probably considered the primary factor in quantum yield reduction for Trp in proteins. Proton transfer from a terminal ammonium group to Trp can reduce quantum yield,^{15–19} but in proteins, where amide groups predominate, quenching occurs by electron transfer from the ring to an amide.^{10,18,20–24} Charge transfer quenching involving residues is also possible.^{18,24,25}

The protein environment of a single tryptophan can be very complex as many residues, charged or nonpolar, as well as backbone amides may be within a 4 Å radius of interaction with the fluorescent indole ring. In order to reduce the potential number of groups affecting quantum yield, we chose to examine the fluorescence characteristics of the Lys-Trp dipeptide in all possible charge states. As in previous studies of Trp

dipeptides,^{26,27} we employ quantum mechanical (QM) calculations and molecular dynamics (MD) simulations to provide information on the dominant molecular conformations. We examine these in tandem with fluorescence lifetimes, steady-state fluorescence emission spectra, and quantum yield determinations for all Lys-Trp charged species. As before, we find that backbone-ring interactions for all Lys-Trp species are controlled by the dihedral angle, chi 1, and that three angles predominate: 60°, 180°, and 300°. Digital switching between the chi 1 conformers is also observed. Unlike past studies, however, terminal amine cation–indole interactions are all but absent and so cannot be used to explain spectroscopic features for the cationic species. The van der Waals contacts for Lys-Trp cations are not qualitatively or quantitatively different from those observed for the zwitterion or anion species, and so these also cannot account for the precipitous decrease in cationic quantum yield and shorter fluorescence lifetimes. In addition, the relative stability of the 60°, 180°, or 300° chi 1 rotamers is unlikely to be a factor because, unlike the previous Trp-Glu

Received: April 4, 2014

Revised: May 29, 2014

Published: June 1, 2014

study,²⁷ they do not display recognizably significant differences in their stability.

These spectroscopic features remain inexplicable until the evidence of exoring negative charge on $C_{\beta'}$ and the possibility of alternate indole resonance structures and changes in aromaticity are considered. Therefore, we examine QM-MD-derived indole ring isosurfaces,^{28,29} which show the ground state π -electron density at specific distances from the ring plane. This exercise reveals a trend in decreased ring charge density and delocalization (i.e., loss of aromaticity) with increased positive charge on the peptide backbone and Lys residue, which is paralleled by decreased quantum yield and fluorescence lifetime. A dramatic decrease in the intensity is seen above the pK_a of the indole amine, which is also predicted by the notable alteration in isosurface charge distribution or aromaticity. In the absence of isosurface data for proteinaceous Trps, observed extremely low quantum yield is explained with similar changes in aromaticity for tryptophans that are hydrogen bonded at the indole amine. This is expected to give rise to the nonaromatic π -electron density distribution observed for the deprotonated indole tautomer.

The association between ground state conformation and fluorescence of aromatic compounds, including indole derivatives, was first studied in 1970 by IB Berlman.³⁰ More recently, the optical and electronic properties of aryl-substituted benzobisoxazoles³¹ and pyrenes³² have been tuned via substituents that affect the π -conjugated electrons. These substituents mainly affect the highest occupied molecular orbital (HOMO, ground state) and lowest unoccupied molecular orbital (LUMO, first excited fluorescent state), but it has been demonstrated that the HOMO can be tuned without significantly affecting the LUMO. Thus it is found that the ground state can tune fluorescence properties. These results further support our finding that the ground state isosurfaces of Lys-Trp dipeptide species correlate with quantum yield and fluorescence lifetimes because for indole, the HOMO is the predominant ground state for the fluorescing transition dipole, 1L_a .³³ In comparing the isosurfaces of the Lys-Trp dipeptide species, we find that the electron density distribution for the isosurfaces of the highly fluorescent zwitterion and -1 charged species resemble that for the calculated HOMO molecular orbital for indole, which is the dominant ground state orbital for the fluorescent transition dipole, 1L_a .^{33,34}

This is the first time that changes in tryptophan quantum yield and lifetimes have been linked to changes in ring aromaticity.

RESULTS

Fluorescence Emission and Quantum Yield. The fluorescence emission maximum for each Lys-Trp species is given in Table 1. The maxima range in value from 355 to 375

Table 1. S1 Absorption Band and Fluorescence Emission Maxima with Quantum Yield for Lys-Trp dipeptide Species

pH	absorption maximum (nm)	emission maximum (nm)	quantum yield	R^2
1.5	279	355	0.032	0.97
5.3	279	357	0.059	0.99
9.3	279	358	0.14	0.93
11.0	280	359	0.14	0.95
13.0	283	375	0.014	0.89

nm. These values are red-shifted relative to the emission maximum for aqueous Trp at 350 nm. The quantum yield measurements require recording absorption spectra for the Lys-Trp dipeptides. The S₁ absorption band maxima are included in Table 1. Lys-Trp species have maxima ranging from 279 to 283 nm.

The quantum yields for Lys-Trp charged species fall into two sets: a low quantum yield for (Lys-Trp)²⁺ (pH 1.5, QY = 0.032), (Lys-Trp)⁺ (pH 5.3, QY = 0.059), and (Lys-Trp)⁻ with deprotonated indole amine (pH 13.0, QY = 0.014), and a higher quantum yield, QY = 0.14, identical to that of L-Trp,³⁵ for Lys-Trp zwitterion (pH 9.3) and (Lys-Trp)⁻ (pH 11.0). Protonation at the indole amine at pH 1.5 is not a consideration because Trp quantum yield is already at a minimum at this pH while the indole minimum is at a pH < 1.³⁶ In a study of Tyr mutants at positions 8 and 10 of a 12-mer β -hairpin peptide,¹⁴ the quantum yield of the adjacent Trp dropped to ~ 0.02 at a pH above the Tyr pK_a . This suggests formation of a TyrO⁻, indole amine hydrogen bond, where partial deprotonation of the indole amine results in a very low QY as for the Lys-Trp dipeptide at pH 13.0 (above the pK_a of the indole amine).

Fluorescence Lifetime Measurements. Two sets of fluorescence lifetimes are given in Table 2. The first set of

Table 2. Fluorescence Lifetime Decay Analysis for Lys-Trp Dipeptide Species

pH	τ (ns)		A (%)		χ^2	
1.5	—	—	—	—	1.03 ^a	—
	0.589 ^a	0.769 ^b	71 ^a	—		
	1.21	—	29	—		
5.3	0.629	1.43	0.538	1.44	48	15
	—	—	1.45	—	79	1.05
	2.17	—	3.52	52	6.0	—
9.3	2.44	3.15	2.08	2.98	55	28
	4.01	—	3.25	45	71	1.02
	—	—	9.28	—	1.1	—
11.0	—	—	0.6773	3.66	—	6.4
	1.78	2.84	2.72	45	72	1.21
	3.70	—	7.89	55	21	1.19
13.0	—	—	0.904	1.03	98	—
	—	—	8.85	—	1.6	1.26

^aFit to RLBL data. ^bItalicized numbers are amplitude-weighted average lifetimes.

lifetimes, τ (set 1), found in the first column of Table 2, is derived from measurements made on the Ti:sapphire-pumped laser system (ca. 45 ps instrument response function, fwhm), while the second set (set 2) derives from the photodiode system (1.47 ns instrument response function, fwhm). The fluorescence decay datum obtained on the Ti:sapphire instrument for the Lys-Trp species at pH 1.5 is shown in Figure S1 of the Supporting Information, while the data obtained from both instruments for the species at pH 11.0 are shown in Figures S2 and S3 of the Supporting Information. The fitted lifetime decays and residuals are also shown. Fluorescence decay analyses found two or three lifetimes for each Lys-Trp species (Table 2). This is true for both data sets.

A subnanosecond lifetime dominates the results for (Lys-Trp)²⁺ (pH 1.5): 0.589 ns (amplitude = 71%), set 1. The average lifetime for (Lys-Trp)²⁺ is 0.769 (Table 2, italics). A reliable fit to lifetime decay data from the photodiode system

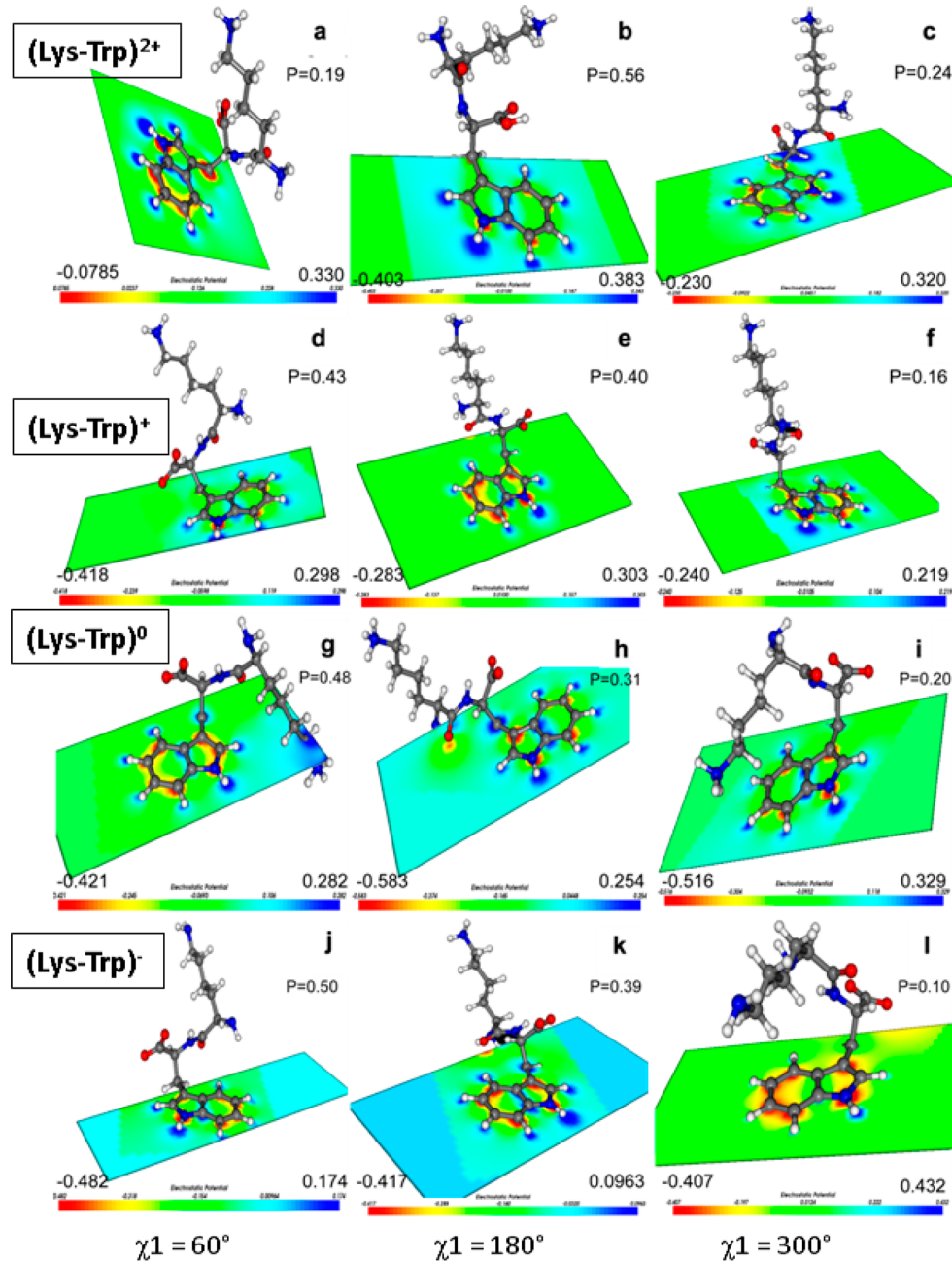


Figure 1. Electrostatic potential surfaces of the indole plane for all lowest energy Lys-Trp species. All conformers are arranged in order of increasing chi 1 angle from left to right: 60°, 180°, and 300°. The probability, P , of each conformer is indicated. (a–c) (Lys-Trp)²⁺, (d–f) (Lys-Trp)⁺, (g–i) (Lys-Trp)⁰, (j–l) (Lys-Trp)⁻. Significant electrostatic interactions ($< 4 \text{ \AA}$) are given in Table S1 of the Supporting Information. The electrostatic potential scale at the bottom of each conformer is in atomic units, with red indicating negative charge and blue, positive charge.

could not be obtained. Two lifetimes of equivalent amplitude comprise the set 1 results for (Lys-Trp)⁺ (pH 5.3, Table 2): 0.629 and 2.17 ns. Set 2 is dominated by similar lifetimes with a different amplitude distribution: 0.538 ns ($A = 15\%$) and 1.45 ns ($A = 79\%$). The average lifetimes for (Lys-Trp)⁺ in both data sets are 1.4 ns, noticeably longer than that for the (Lys-Trp)²⁺ species. Both sets of lifetimes for Lys-Trp zwitterion (pH 9.3) are dominated by two ns lifetimes of magnitude $2 < \tau < 4$ but amplitudes vary. Amplitude is nearly evenly split between lifetimes of 2.44 and 4.01 ns in set 1, while a lifetime of 3.25 ns dominates set 2 ($A = 71\%$). The average lifetime in both data sets is 3 ns, which is significantly longer than that of the (Lys-Trp)⁺ species. The two lifetimes of set 1 for (Lys-

Trp)⁻ (pH 11.0), 1.78 and 3.70 ns, are shorter than those for the Lys-Trp zwitterion in set 1, but the average lifetime is the same (3 ns). Set 2 lifetimes consist mainly of a dominant ($A = 72\%$) lifetime of 2.72 ns and a longer lifetime of 7.89 ns ($A = 21\%$) with an average lifetime of 4 ns. The lifetime measurement for the indole conjugate base of (Lys-Trp)⁻ (pH 13.0) (i.e., the indole amine is deprotonated) is dominated ($A = 98\%$) by a 0.9 ns lifetime. The minor lifetime ($A = 2\%$) component is 8.85 ns. The average lifetime is 1.0 ns.

MD Simulation. Conformers Defined by the Dihedral Angle, chi 1. As for Trp-Gly, Gly-Trp,²⁶ and Trp-Glu²⁷ dipeptide species, molecular dynamics simulations for the Lys-Trp dipeptide species show that the relative position of the

backbone to the indole ring is defined by the chi 1 dihedral angle. Again, three chi 1 dihedral angle distributions define this orientation. These distributions are centered at ca. 60°, 180°, and 300°. The simulated time course of the chi 1 angle changes for four of the Lys-Trp species are given in Figures S4–S7 of the Supporting Information. As for other Trp dipeptides,^{26,27} conformational switching between chi 1 angles can generally be described as digital. That is, the molecule resides at or near one of the characteristic chi 1 angles before switching instantaneously (ca. 1 fs) to another of the preferred chi 1 angles.

Probability Distribution of chi 1 Dihedral Angle Conformers. The chi 1 = 300° conformation is generally the most disfavored for all Lys-Trp charged species while the chi 1 = 60° conformation is the most favored by all species except (Lys-Trp)²⁺. The lowest energy conformers for Lys-Trp dipeptide charged species are shown in Figure 1 along with their probability, and the electrostatic potential (in atomic units) through the indole plane. All stabilizing and destabilizing intramolecular backbone–indole ring interactions within 4 Å are included in Table S1 of the Supporting Information, although the strength of these interactions is not included. Generally, ring-backbone attractive interactions are balanced by an equal number of repulsive interactions. Intramolecular backbone–backbone interactions are given in Table S2 of the Supporting Information. The atomic labeling used to describe these intramolecular interactions is given in Figure 2.

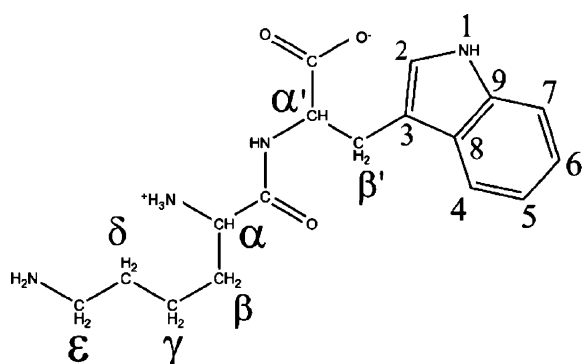


Figure 2. Atomic labeling of the Lys-Trp dipeptide in the zwitterion state.

Common Features of Lys-Trp Lowest Energy chi 1 Conformers. The lysine residue is usually not found in the vicinity of the indole ring (Figure 1) except for the (Lys-Trp)²⁺ chi 1 = 60°, (Lys-Trp)⁰, and (Lys-Trp)⁻ chi 1 = 300° conformers. For these conformers, the probability is low (10–20%). The general disposition of the lysine residue in the remaining conformers is one of an extended chain positioned far from the indole plane. In general, ring-backbone stabilizing interactions are balanced by destabilizing interactions at similar interatomic distances for most Lys-Trp conformers (Table S1 of the Supporting Information). These interactions support the idea that backbone–ring orientation is driven by steric hindrance rather than electrostatic interactions. Such destabilizing interactions provide for the increased frequency of chi 1 angle switching between the three dominant angles and, therefore, the roughly equal probability of the major Lys-Trp conformers. Interaction of the N-terminal amine cation with the indole ring, observed in Trp-Gly, Gly-Trp,²⁶ and Trp-Glu²⁷ charged species, is observed only in the (Lys-Trp)⁺ chi 1 = 60° conformer. Lys-Trp backbone conformations are stabilized by

hydrogen bonds between backbone charged groups (Table S2 of the Supporting Information).

Chi 1 Conformer Ring-Backbone Electrostatic Interactions. For the sake of brevity, only the conformers with higher probability are discussed. For all (Lys-Trp)²⁺ conformers (Table S1 of the Supporting Information), there are 19 favorable ring-backbone interactions within 4 Å. The chi 1 = 180° conformer ($P = 56\%$) is stabilized by four interactions of the C-terminal carboxylic acid hydroxyl group with indoles C₃, C₄, C₄-H, and C₉. The lower probability ($P = 24\%$) chi 1 = 300° conformer is stabilized by peptide carbonyl and amine interactions with the ring. The peptide NH is electrostatically attracted to C₂ and C₃, and the peptide carbonyl is positioned 2.83 Å from the indole C₂ hydrogen. There are also 19 favorable ring-backbone interactions within 4 Å for all (Lys-Trp)⁺ conformers (Table S1 of the Supporting Information). Only the chi 1 = 60° conformer ($P = 43\%$) shows ring interaction with the terminal amine cation. Peptide amide and terminal COOH interactions are also present. The chi 1 = 180° ($P = 40\%$) conformer only shows three terminal COOH–ring interactions and one peptide carbonyl interaction. The (Lys-Trp)⁰ conformers have 29 favorable ring–backbone interactions. For the chi 1 = 60° conformer ($P = 48\%$), interactions with the terminal COO⁻ are favored over those with the peptide carbonyl and amine. The 180° conformer ($P = 31\%$) has four attractive interactions with the terminal COO⁻. The (Lys-Trp)⁻ conformers partake in 15 favorable ring–backbone interactions. The chi 1 = 60° conformer ($P = 50\%$) has numerous ring interactions with the peptide carbonyl and amine and the terminal carboxylate. The chi 1 = 180° conformer ($P = 39\%$) has only a single ring interaction each with the terminal carboxylate and the peptide carbonyl. While a pattern for charged species' backbone–indole ring interactions is difficult to distinguish, we note that a terminal NH₃-amide O hydrogen bond is peculiar to conformers for the positively charged species (Table S2 of the Supporting Information).

Isosurfaces Reveal Differing Patterns of π -Electron Delocalization. Electron density isosurfaces ranging from 0.02 to 0.30 in increments of 0.01 were generated for the indole ring of Trp in each of the conformers for five Lys-Trp species. Isosurfaces where negative charge first appears over the indole ring are given in Figure 3 for one low-energy chi 1 conformer for each dipeptide charged species. For all charged species, the isosurface shown represents the charge distribution for one or more of the remaining two conformers of that charged species. A color scale for the associated charge is shown above each isosurface. Note the progressive shift of the zero charge point to the blue end of the scale as negative charge on the dipeptide increases. Where isosurface charge distribution varied for a conformer, that isosurface is represented by an inset structural model. Isosurfaces not illustrated are included in Supporting Information as slide files of isosurfaces up to an isosurface value of 0.15. The pattern of charge density changes for each conformer is outlined below. Note that isosurface values increase as distance from the ring decreases.

Weak π -Electron Density Concentrated at Indole Ring Periphery in (Lys-Trp)²⁺ and (Lys-Trp)¹⁺. Π -Electron density (-0.00049) first appears at C₄–C₇, along the N–C₂ bond and at C_{β'} at the 0.08 isosurface for the chi 1 = 60° conformer of (Lys-Trp)²⁺ (Figure 3a). The remaining ring carbons, C₃, C₈, and C₉, are positive at this isosurface value (0.195). At isosurface value 0.11, C₇ and C_{β'} are the most negative (-0.0631); C₃, C₈, and C₉ remain positive (ca. 0.200);

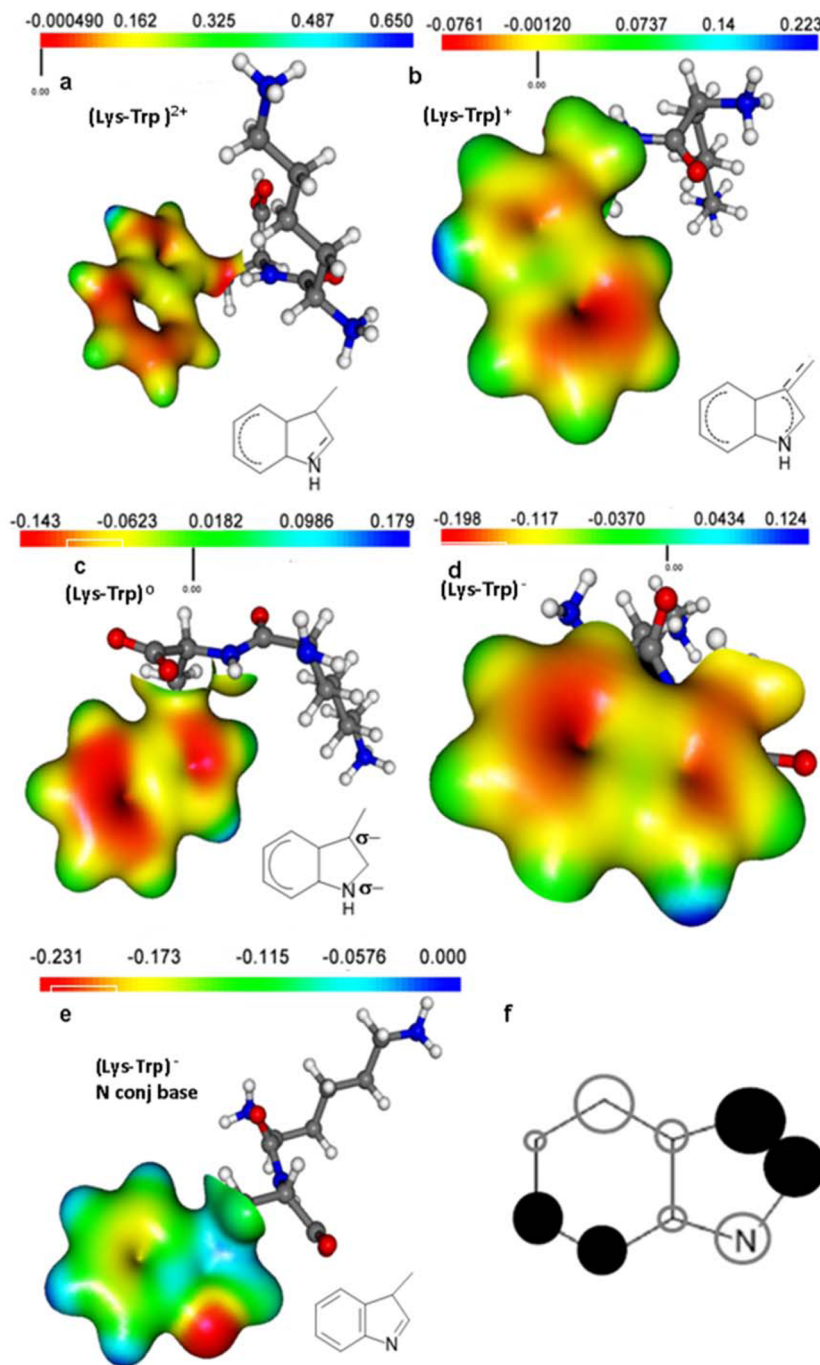


Figure 3. Charge density isosurfaces for the indole of each Lys-Trp charged dipeptide. The color-coded electrostatic potential scale, with zero potential marker, is given above each figure. The inset figures are models for the isosurface of conformers not represented by the color images. Solid contour lines represent ring position of high electron density (-10^{-1}) while dashed lines represent ring position of weak electron density (less than -10^{-2}). Where no contour line is present, the isosurface show zero or positive charge. (a) $(\text{Lys-Trp})^{2+}$, $\chi_1 = 60^\circ$, 0.080 isosurface; also represents the 0.050 isosurface of the 300° conformer. Inset: $\chi_1 = 180^\circ$, 0.060 isosurface (b) $(\text{Lys-Trp})^+$, $\chi_1 = 180^\circ$ and 300° , 0.020 isosurface. Inset: $\chi_1 = 60^\circ$, 0.020 isosurface. (c) $(\text{Lys-Trp})^0$, $\chi_1 = 60^\circ$ and 180° , 0.020 isosurface. Inset: $\chi_1 = 300^\circ$, 0.02 isosurface. (d) $(\text{Lys-Trp})^-$, $\chi_1 = 60^\circ$, 0.020 isosurface; represents 0.020 isosurface of all anionic conformers. (e) $(\text{Lys-Trp})^-$ /Ind N conj base, $\chi_1 = 60^\circ$, 0.02 isosurface. Inset: tautomer structure. (f) Highest occupied molecular orbital (HOMO) for indole in vacuum calculated via an *ab initio* method (MP2/6–31G*) image adapted from ref 45. This is the major ground state orbital for the ${}^1\text{L}_\alpha$ transition, the primary fluorescing transition in indole.

remaining ring atoms have close to zero charge. At an isosurface value of 0.15, the $\text{C}_{\beta'}$ carries more negative charge (-0.170) than any ring atom except nitrogen.

Isosurfaces for the $\chi_1 = 300^\circ$ conformer of $(\text{Lys-Trp})^{2+}$ share this charge distribution. Π -Electron density first appears at isosurface 0.05 (-0.00190) from C_4-C_7 . At isosurface 0.08,

C_4-C_7 and $\text{C}_{\beta'}$ are at a charge of -0.0200 while the $\text{N}-\text{C}_2$ bond is less negative. Ring carbons, C_3 , C_8 , and C_9 , are positive (ca. 0.100). At an isosurface value of 0.13, C_4 , C_7 , and $\text{C}_{\beta'}$ are most negative (-0.112); C_3 , C_8 , and C_9 remain positive.

The pattern of π -electron density for the $\chi_1 = 180^\circ$ conformer of $(\text{Lys-Trp})^{2+}$ differs (Figure 3a, inset). C_4-C_7 and

the N—C₂ bond first appear negatively charged (-0.000157) at isosurface 0.06, but C_{β'} is positive, as are C₈ and C₉ (ca. 0.15). At isosurface 0.12, negative charge (-0.0623) can be found at C₄—C₇ and at the N—C₂ bond, but the remaining ring carbons and C_{β'} are positive. For all (Lys-Trp)²⁺ conformers, the ring π -electron density is not uniform over the indole ring; the aromaticity would be diminished.

For all (Lys-Trp)⁺ conformers, a weak π -electron density (-0.076 to -0.03) appears at an isosurface value of 0.02 (Figure 3b), further from the indole ring plane than in (Lys-Trp)²⁺. C₈ and C₉ remain positive (<0.1). For the chi 1 = 60° conformer of (Lys-Trp)⁺ (Figure 3b, inset) at isosurface 0.02, the weak negative charge extends to C_{β'}, while for the chi 1 = 180° and chi 1 = 300° , it does not (Figure 3b). For this cation, the ring π -electron density lacks uniformity over the entire indole molecule, and the aromaticity is still diminished over most of the isosurfaces studied for this charge species.

Π-Electron Density Spans the Indole Ring in (Lys-Trp)⁰ and (Lys-Trp)⁻. For all (Lys-Trp)⁰ conformers, π -electron density (ca. -0.15 — -0.10) appears at C₄—C₇ at an isosurface value of 0.02 (Figure 3c). C₈, C₉, and C_{β'} are weakly negative in the 60° and 180° conformers only. The N—C₂—C₃ portion of the pyrrole ring also has relatively high π -electron density in the 60° and 180° conformers (Figure 3c). As the isosurface value increases (where the distance is closer to the ring plane), π -electron density concentrates at C₄—C₇ and N—C₂—C₃, while C₈ and C₉ become less negative.

The π -electron density distribution for the 300° conformer (Figure 3c, inset) deviates from the above pattern in that N and C₃ carry a charge of ca. -0.1 , but C₂ is only slightly negative. As the isosurface value increases, C₃ carries the greatest ring charge for the 300° conformer.

All ring atoms of all (Lys-Trp)⁻ conformers carry a π -electron density of ca. -0.2 to -0.1 at the 0.02 isosurface (Figure 3d). For both the (Lys-Trp)⁰ and (Lys-Trp)¹⁻ species, the π -electron density is continuous even at the 0.020 isosurface, conferring aromaticity to these species.

(Lys-Trp)⁻/Ind N Conj Base. Deprotonation of the indole amine is predicted to result in π bond migration (tautomerization) from C₂—C₃ to N—C₂.^{37,38} While the pK_a of indole in dimethyl sulfoxide is 21, and substitution of C₃ with N reduces pK_a to only 16.4,³⁹ Osysko and Muino similarly found that the quantum yield of aqueous Trp, Trp-Asp, and Trp-Arg dipeptides dropped precipitously above pH 11.¹² They attributed the quantum yield decrease to deprotonation of the indole amine, as crossing of the potential energy surface for the nonradiative Rydberg state, A'' ($\pi\sigma^*$), with those of the fluorescent ¹L_a($\pi\sigma^*$) and ground states occurs as a function of the indole N—H distance.⁴⁰

The 0.02 isosurface for the (Lys-Trp)⁻/Ind N conj base (Figure 3e) indeed shows -0.17 to -0.1 π -electron density around the benzyl ring and at C₂. The pyrrole N has the highest negative charge (-0.2), while C₃ is only weakly negative (less than -0.06). A different pattern of π -electron density on the indole ring results for this species. The tautomer structure for indole with deprotonated pyrrole is given in the inset of Figure 3e.

NMR Spectroscopy Insensitive to Aromaticity Changes. NMR spectroscopy of Lys-Trp at pH 1.5 and 12.5 was carried out to confirm the changes in aromaticity observed in isosurfaces. Chemical shifts for indole C₂, C₄, and C₇ hydrogens were 0.5 ppm, which is within the standard error on peak positions in proteins.⁴¹ Therefore, NMR is insensitive to the

diminished aromaticity found in the isosurface studies, unlike fluorescence quantum yield.

Other Measures of Aromaticity. The harmonic oscillator measure of aromaticity (HOMA)⁴² and nucleus-independent chemical shifts method (NICS)⁴³ were not appropriate for our molecules and did not yield values that tracked with changes in quantum yield or fluorescence lifetime.

The HOMA measure of aromaticity⁴² is better-suited to predicting aromaticity in different extended ring systems where there are substantial changes in bond length and the number of rings changes. For example, for perylene, the center ring HOMA index is 0.140, whereas the highest index for an outer ring is 0.842.⁴² The dipeptides here do not constitute such a system. The difference between our dipeptides is in the charge on the backbone and the change in orientation of the backbone with respect to the indole ring. The variation in HOMA aromaticity index for the indoles in the LysTrp dipeptides in different charge states is small: 0.829–0.845, and does not track with the quantum yield or fluorescence lifetimes. A similar result is expected for Randic's method of conjugated circuits.⁴⁴

The NCSI data is mainly for the deshielding effects of the electrons. This is an indirect effect of the electron density and configuration within the molecule. The absorption and fluorescence, however, relate to the state of the electronic energy levels and are more directly affected by the electron density in the indole ring.

The NCSI information tells very little, if anything at all, about the aromaticity differences. It does show a very slight increase of aromaticity for the (Lys-Trp)⁻ over the (Lys-Trp)²⁺ when not in the plane of the nuclei of the indole ring, but a slight decrease of aromaticity when in or very close to the atoms of the indole ring. The calculated differences between the two species might be small enough to be indistinguishable experimentally.

DISCUSSION

A common pattern is found for Lys-Trp species quantum yields and fluorescence lifetimes. While the number of lifetimes for each data set (Table 2) and species varies, lifetimes with the highest amplitude have a match across the two sets for each species when available, and weighted average lifetimes are similar for both data sets. The dominant lifetime for (Lys-Trp)²⁺ (pH 1.5, Table 2) is 0.589 (A = 71%). A 10^{-1} ns lifetime is also found for (Lys-Trp)⁺ (pH 5.3, Table 2) in both data sets, but the amplitude of this component has diminished (A = 48% and 15%). Instead, 10^0 ns lifetimes dominate fluorescence decays. With the loss of a proton on the N-terminal amine, lifetimes are dominated by two 10^0 ns values (Table 2, pHs 9.3 and 11.0). When the indole amine is deprotonated (Table 2, pH 13.0), a 10^{-1} ns lifetime once again dominates (A = 98%), and there is a minor (A = 2%) 9 ns component. Weighted average lifetimes result in a 0.77 ns lifetime for (Lys-Trp)²⁺, 1.0 for (Lys-Trp)⁻/Ind N conj base, and a 1.4 ns lifetime for (Lys-Trp)⁺. Weighted average lifetimes for (Lys-Trp)⁰ and (Lys-Trp)⁻ are all in the 3–4 ns range for both data sets (Table 2).

Quantum yields for these Lys-Trp species follow a similar pattern. Cations, (Lys-Trp)²⁺ and (Lys-Trp)⁺, have low quantum yields of 0.032 and 0.059 (Table 1). The quantum yield for the (Lys-Trp)⁻/Ind N conj base is the lowest obtained, 0.014. The Lys-Trp zwitterion and anion, however, both have quantum yields of 0.14, which is the same value obtained for Trp at pH 7.4. Plotting the weighted average lifetime as a function of quantum yield reveals a linear

relationship for the Lys-Trp species (Figure 4). Such a clear relationship between these fluorescence parameters does not

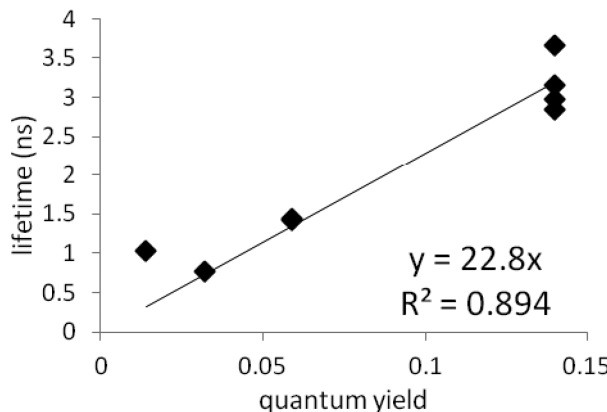


Figure 4. Weighted average lifetime (ns, sets 1 and 2, Table 2) plotted as a function of quantum yield (Table 1) for Lys-Trp species at pH 1.5–13.0. Linear fit plotted with y intercept at $(x,y) = (0,0)$, $R^2 = 0.894$.

exist for single tryptophan proteins.^{7,46,47} This is likely due to the superposition of effects caused by numerous residues for protein tryptophans.

In earlier studies of the Trp-Gly, Gly-Trp, and Trp-Glu species,^{26,27} a terminal amine cation was found in close proximity to the indole ring for several conformers of charged species, which would facilitate proton transfer.²⁴ For the Lys-Trp species studies here, a terminal amine cation in close proximity (3.7 Å, Table S1 of the Supporting Information) to an indole ring is found only for the $(\text{Lys-Trp})^+$ chi 1 = 60° conformer. Favorable van der Waals ring contacts with the peptide amide and/or terminal carbonyl groups provide for possible electron transfer for all four Lys-Trp species below pH 13.^{17,20,24,48,49} Indeed, these van der Waals contacts are most likely a major quenching route for all species, as even the relatively strong fluorescing zwitterion and anion have a diminished quantum yield of 0.14 relative to the high value of 0.34 observed for aqueous 3-methylindole.¹⁷ The cationic Lys-Trp species are distinguished by terminal amine cation–amide oxygen hydrogen bonds. Theoretical⁵⁰ and spectroscopic⁵¹ studies of *N*-acetyl tryptophan amide (NATA) and its methyl amide (NATMA) have revealed an LE excited state along a peptide backbone hydrogen bond, which acts as an excitation conduit from the fluorescent ${}^1\text{L}_\alpha$ state to charge transfer (CT) deexcitation. The reduced and asymmetric π -electron density for the indole in these Lys-Trp cationic species may constitute a telltale for such a CT state.

Quantum mechanical isosurface charge distribution for Lys-Trp peptides shows changes in ring aromaticity with molecular charge and pK_R . One factor that has not been considered is the effect of molecular charge on distribution of ring π -electron density. The isosurface charge distribution on the indole ring for $(\text{Lys-Trp})^{2+}$ conformers reveals a π -electron density that is diminished and weak, extending above the ring plane only to isosurface 0.05–0.08 (i.e., near the ring plane) (Figure 3a). Furthermore, charge density does not encircle the ring, and charge density is found off the ring on C_{β} , suggesting that a resonance structure with off-ring conjugation is favored. Positive charge on the backbone favors off-ring π -electron density. This results in greatly diminished aromaticity for the

$(\text{Lys-Trp})^{2+}$ species, which increases the ground state energy of the indole ring, placing it closer to the LE origin.⁵⁰ Short-lived deexcitation pathways, such as the LE to CT transition, are favored over the nanosecond fluorescence emission route. A low quantum yield (0.032) and a predominant subnanosecond lifetime (Table 2) is characteristic of nonaromatic compounds and are observed here for the $(\text{Lys-Trp})^{2+}$ species.

A small increase in ring charge density is found for $(\text{Lys-Trp})^+$ conformers in that weak charge is extended out to the 0.02 isosurface (Figure 3b), but the π -electron density is not continuous about the ring here either. Charge density along the C_3-C_{β} bond is observed for the 60° conformer, suggesting that exoring conjugation also contributes to the π -electron density distribution. Quantum yield is also low for $(\text{Lys-Trp})^+$ (0.059), but lifetimes have increased with an average lifetime of 1.4 ns. A smaller positive charge on the dipeptide allows for an increased stabilization of the excited state and, therefore, a small increase in fluorescence lifetime.

The Lys-Trp zwitterion 0.02 isosurface charge density is stronger still and continuous about the ring (Figure 3c). Exoring charge density does not appear to be a part of the π -electron distribution as the isosurface shows C_{β} to be positively charged. The quantum yield, 0.14, is identical to that for Trp in water. An average lifetime of 3 ns results.

The π -electron density distribution on the indole ring for the $(\text{Lys-Trp})^-$ conformers is strong and relatively uniform at the 0.02 isosurface (Figure 3d). Aromaticity prevails, and the quantum yield is the same as for aqueous Trp. Negative charge on the peptide should stabilize the excited state where electrons are at a further distance from the indole plane and, therefore, favor the long-lived fluorescence emission process. Slightly longer average lifetimes of 3–4 ns are found (Table 2). Deprotonation of the indole amine at pH 13.0 again disrupts the ring π electron distribution (Figure 3e). There is little electron density at C_3 and high electron density at the pyrrole nitrogen. The result is that quantum yield drops to 0.014 and the average lifetime is shortened to 1.0 ns. Positive charge on C_3 and the pyrrole ring is consistent with the dissociative state, $\pi \rightarrow \sigma^*$,⁵¹ which is predicted to cross the ${}^1\text{L}_\beta$ energy function just above the indole NH stretch vibration.⁵⁰

Accounting for a 10-fold Decrease in Trp Quantum Yield in Proteins: Loss of Aromaticity. Our finding of loss of aromaticity for Lys-Trp cationic and deprotonated indole amine species provides a plausible explanation for the drop in quantum yield from 0.14, observed for aqueous Trp, to the minima of 0.01 observed in proteins. For the cationic species, backbone and Lys residue positive charge can shift fluid ring π -electron density toward the exoring C_{β} , as shown by the isosurfaces (Figure 3, panels a and b). The ground state isosurfaces for the cationic Lys-Trp species (Figure 3, panels a and b) are lacking in π -electron density at the C_2 or C_3 ring atoms characteristic of the fluorescent ${}^1\text{L}_\alpha$ ground state, the HOMO (Figure 3f). Concomitantly, these same positive charges destabilize the electronic excited state, disfavoring the longer, nanosecond process of fluorescence emission. For the deprotonated indole amine species, the pyrrole C_2-C_3 double bond is shifted to N–C₂ and electron density is concentrated at the pyrrole nitrogen, a tautomer is favored (Figure 3e, inset).^{37,38} The corresponding isosurface (Figure 3e) shows a very distorted ring π -electron distribution, which is also very different from the fluorescent ${}^1\text{L}_\alpha$ ground state. Loss of aromaticity favors a nonradiative process of deexcitation and a lower quantum yield, as found in the fluorescence spectra.

Loss of Aromaticity Can Account for Low Quantum Yield in Proteins. This line of reasoning can be applied to the pK_a -dependent quantum yield results for mutants of a dodecamer β -hairpin peptide, where residues flanking either face of a single tryptophan were mutated.¹⁴ Plots of fluorescence yields follow the pK_a for the Trp-flanking residue and the associated molecular charge. If the flanking residue is Asp ($pK_R = 3.65$), Glu ($pK_R = 4.25$), Cys ($pK_R = 8.18$), or His ($pK_R = 6.00$), quantum yield is higher when the residue is in the anionic state and lower when the residue is protonated. This is readily explained by the diminished indole aromaticity found in the presence of positive charge as found here for Lys-Trp cations. When the flanking residue is Tyr, the quantum yield for the β -hairpin peptide follows a different rule with respect to the residue pK_R , as discussed below.

Hydrogen Bonding at the Indole Amine Favors a Tautomer. The strength of a concept rests in how well it explains the observed phenomena. As hydrogen bonding at the indole amine favors Trp tautomerization (Figure 3e, inset), and the C_3 tautomer has been shown to be of lowest energy,³⁸ it is reasonable to expect that indole aromaticity and, therefore, quantum yield, would be affected, as observed here for Lys-Trp at pH 13. This scenario has, in fact, been documented in studies of Trp fluorescence in proteins. The pH-dependent fluorescence yields for Trp in the β -hairpin Phe10Tyr and Ala8Tyr mutants follow Tyr $pK_R = 10.07$.¹⁴ The Trp fluorescence yields drop to ca. 0.02 when Tyr OH is deprotonated. Examination of the NMR structure for the Phe10Tyr mutant provided therewithin shows that $TyrO^-$ —Trp pyrrole NH hydrogen bonding is possible. Hydrogen bonding at the indole amine favors an indole tautomer-like structure and, therefore, a low quantum yield is expected and observed for the β -hairpin mutant.

In a study of the pH-dependence of fluorescence for the W126Y/W158Y/Q105H single Trp mutant of T4 lysozyme,⁵² average lifetime falls from 3 to 2 ns and fluorescence yield decrease 3-fold as pH rises above His pK_a . This result is in disagreement with the low Trp quantum yields that have been associated with protonated His.^{53–55} As His replaces the wild-type Gln105 in mutant T4 lysozyme, which crystal structure shows is hydrogen bonded to the Trp138 indole amine,⁵⁶ similar hydrogen bonding by the His anion was indicated.⁵² Once again, a Trp tautomer would be favored, leading to the observed lower fluorescence. The evidence supports a loss of aromaticity and a tautomer structure for the T4 lysozyme mutant Trp138 above His pK_R as observed here for Lys-Trp at pH 13.0.

Finally, we examine the low quantum yield obtained for members of the homeodomain element from the family of homeotic proteins.⁸ The single Trp human homeodomain, Pbx-1, with an extremely low quantum yield,⁵⁷ contains a Trp25 pyrrole NH–Glu39 O_E hydrogen bond of length 2.37 Å, as revealed by NMR.⁵⁸ *Drosophila* homeodomain antennapedia C39S mutant, which contains two Trps, shows very low fluorescence emission with an average folded lifetime of 1.30 ns and a 4-fold increase in fluorescence emission upon unfolding.⁸ The NMR structure for this homeodomain shows a Thr13 residue O–Trp48 pyrrole NH hydrogen bond distance of 1.97 Å (PDB 1hom). Other *Drosophila* homeodomains, Ubx and Eng, also exhibit very low fluorescence yield;⁸ however, NMR or crystal structures free of the structure-altering DNA adduct are not available, and so hydrogen bonding at the indole amine cannot be checked. The concurrence of these results supports

the concept of indole ring π -electron density redistribution via hydrogen bonding at the indole amine and a drastic reduction in Trp quantum yield as a result of loss of aromaticity that this electron density change causes.

CONCLUSIONS

The Lys-Trp dipeptide was studied both spectroscopically and *in silico* in pH-induced charge states ranging from 2^+ to 1^- and deprotonated at the indole amine. Quantum yields for the Lys-Trp dipeptide species followed a linear relationship with fluorescence lifetime averages. As for Trp-Gly, Gly-Trp, and Trp-Glu dipeptides, the chi 1 dihedral angle is found to control the relative disposition of the backbone to the indole ring. Simulations for Lys-Trp cations did not reveal a predilection for the terminal amine cation to interact with the indole ring. The absence of backbone and Lys residue interaction with the indole ring in all charge states necessitates some explanation for the quantum yield and fluorescent lifetime decreases observed when Lys-Trp is in the cationic state or when the indole amine is deprotonated. A feasible explanation is provided by the quantum mechanically derived isosurfaces of the indole ring, which reveal molecular charge- and pK_R -associated changes in π -electron density that are tantamount to changes in ring aromaticity. It is noteworthy that the isosurface charge distributions for the higher quantum yield Lys-Trp zwitterion and anion most closely matches that of the calculated indole HOMO, which is the main ground state for the fluorescing 1L_a transition dipole moment. Thus it is not necessary to calculate individual molecular orbital charge distribution as the isosurface represents the sum charge distribution, which can be compared to the ground state of the fluorescing 1L_a transition dipole moment. At pH 13, where the indole amine is deprotonated, a tautomer is favored that concentrates π -electron density at the nitrogen, and consequently the quantum yield is extremely low (0.014). The ground state does not resemble that for the 1L_a transition dipole. In the absence of isosurfaces for proteinaceous Trps, verification of a correlation between extremely low Trp quantum yield and loss of aromaticity is found in extremely low fluorescing Trp-containing proteins where hydrogen bonding at the indole amine can be demonstrated. The expected indole π -electron charge distribution is like that observed here for Lys-Trp with deprotonated indole amine. It is noteworthy that these changes in aromatic character are not found using ordinary proton NMR. The electron density has a direct effect on the energy states that govern fluorescence phenomena, whereas the effect of aromaticity on the deshielding of neighboring protons is an indirect effect. Here we see that fluorescence spectroscopy can be a more sensitive probe of the aromatic character of the indole ring electron density distribution.

EXPERIMENTAL PROCEDURES

The Lys-Trp dipeptide was purchased from Research Plus, Inc. (Barnegat, NJ) and used without further purification. Aqueous solution pH was adjusted with 1 mM HCl or NaOH solution. The pH was adjusted to 1.5 for (Lys-Trp) $^{2+}$ (fully protonated), 5.5 for (Lys-Trp) $^+$ (additionally, terminal acid deprotonated), 9.5 for (Lys-Trp) 0 (terminal amine deprotonated), 11.5 for (Lys-Trp) $^-$ (lysine deprotonated), and 13.0 for (Lys-Trp) $^-$, indole conjugate base (indole amine deprotonated). L-tryptophan was purchased from Acros Organics (Thermo-

Fisher Scientific, NJ), and 2-aminopyridine was purchased from Alfa Aesar (Ward Hill, MA).

Absorption Measurements. Background corrected absorption spectra were recorded on a Cary 100 Bio UV-vis spectrophotometer (Varian Instruments, Walnut Creek, CA) with a 2 nm slit width, 1 cm path length, and 1 nm interval.

Steady-State Fluorescence Emission Measurements. Fluorescence emission spectra for quantum yield determinations were recorded on a Fluorolog 3 model FL-1000 (Horiba Jobin Yvon, Edison, NJ) fluorometer using an excitation wavelength of 280 nm and a 1 nm interval. The integration time was set to 0.1 s. The slit width matched that of absorption spectrophotometer (2 nm). All concentrations were < 0.01 mM to avoid inner filter effects.

Quantum Yield Determination. Aqueous L-Trp ($QY = 0.14^{35}$) and 2-aminopyridine in 0.1 M sulfuric acid ($QY = 0.60^{59}$) were used as quantum yield standards. Lys-Trp quantum yields were determined by the method given in ref 60. Briefly, the quantum yield of the two quantum yield standards are first determined via reference against each other to ensure confidence in quantum yields measured for the unknown. The integrated fluorescence intensity of each fluorophore is determined from emission spectra at several fluorophore concentrations, all less than 0.01 mM, to avoid the inner filter effect. The integrated intensity is plotted as a function of the measured absorbance at each concentration. A linear fit is calculated, ensuring that the fit line runs through the origin. Obviously, the goodness-of-fit should be close to unity. The slope of the fit is the gradient, G , used in calculation of the quantum yield, QY :

$$QY_x = QY_{st} \left(\frac{G_x}{G_{st}} \right) \left(\frac{\eta_x^2}{\eta_{st}^2} \right)$$

where the subscript, st, signifies the quantities for the quantum yield standard, and x are the quantities for the fluorophore of unknown quantum yield. η is the refractive index for each solution: $\eta = 1.333$ for water and $\eta = 1.334$ for 0.1 M sulfuric acid.⁶¹

Time-Resolved Fluorescence Lifetime Decay Measurement. Fluorescence lifetime measurement of the Lys-Trp dipeptide species, pH 1.5–11.0, was carried out on two different instruments: a commercial instrument that employs a laser diode excitation source with a broad (1.47 ns) instrument response function (Horiba Jobin Yvon, Edison, NJ), and a Ti:sapphire-pumped, lab-built laser system at the NIH-sponsored Ultrafast Optical Processes Laboratory (University of Pennsylvania, Philadelphia, PA). Lifetimes for the pH 13.0 species were measured on the laser diode system only.

The Ti:sapphire-based instrument uses the time-correlated single photon counting method. It provides 300 mW of approximately 800 nm with a repetition rate of 85 MHz. A lab-build beta barium borate-based, third harmonic generator yields the necessary 280 nm excitation pulses. An experimental instrument response function (ca. 45 ps fwhm) was collected from the scattered light off a thin wire, which is necessary for proper deconvolution.⁶² Emission at 340 nm was monitored in a magic angle geometry through a subtractive double monochromator with a microchannel plate-photomultiplier tube (model R2809U, Hamamatsu Photonics, Bridgewater, NJ) connected to a time-correlated single photon counting computer board (model SPC-630, Becker and Hickl, Berlin, Germany).

Excitation was achieved at 280 nm, while emission was monitored at 340 nm in both set of lifetime measurements. The lifetime measurements were duplicated with an instrument of narrower response function (i.e., the Ti:Sapphire system).

Fluorescence Lifetime Decay Analysis. The lifetimes for decays collected on the diode instrument were determined by iterative convolution using the vendor-provided Decay Analysis, DAS6. Details of this method can be found in ref 27. The lifetime decay data acquired on the Ti-sapphire-pumped system were analyzed with the fitting program, FluoFit (Picoquant, Photonics North America, West Springfield, MA).

NMR Measurements. NMR spectra were obtained on a 200 MHz Varian NMR (Agilent Technologies, CA), using MestRe-C v. 2.1.0 (Mestrelab Research, Escondido, CA) for data processing and analysis.

Density Functional Theory Calculations. Gaussian 09⁶³ was used for *ab initio* quantum mechanical (QM) calculations. Details of our method are given in ref 27. As mentioned, the B3LYP density functional theory method and 6-31++g(df,p) basis set were utilized. The polarizable continuum method with implicit water was used. Ground-state QM calculations for the favored chi 1 angles and lowest energy conformation, revealed by molecular dynamics, were performed. Atomic charges were checked against the NBO (natural bond orbital) results and found to be consistent. The main goal of the calculations was to determine the electrostatic potential distribution in the dipeptide, as this gives insight into intramolecular interactions. The Molekel 5.4.0.8⁶⁴ was used for visualization of the peptide species and their isosurfaces. Interatomic distances between atoms participating in electrostatic interactions were measured with gOpenMol.⁶⁵ Isosurface values are not directly proportional to the actual distances from the nuclei, but the relationship between these isosurfaces and the distance from the indole ring can be estimated with the formula of $d = y_0 + Ae^{(-i/t)}$, where d is the distance in Å, $y_0 = 0.370$, $A = 1.105$, $t = 0.07228$, and i is the isosurface value.

Molecular Dynamics Simulation. Simulations were carried out using GROMACS 4.5.3⁶⁶ for all dipeptide species except the indole conjugate base. A cubic box of dimension 1 nm beyond the dipeptide boundary with ~1000 water molecules was utilized. Periodic boundary conditions were applied in three dimensions. 0.5 fs time steps for a total of 20–30 ns were simulated, thus ensuring that all of the chi 1 dihedral angle space was sampled. Additional details of our method are given in ref 27.

ASSOCIATED CONTENT

S Supporting Information

A table of intramolecular backbone–indole ring interaction distances, a table of intramolecular backbone–backbone interaction distances, fluorescence lifetime decay data and fits, molecular dynamics simulation chi 1 distributions over time, and slide files showing indole isosurface charges for all chi 1 conformers of all Lys-Trp charges species up to 0.15 isosurface value. This material is available free of charge via the Internet at <http://pubs.acs.org.org>.

AUTHOR INFORMATION

Corresponding Authors

*E-mail: ase217@nyu.edu. Tel: 718 951 5000, ext 18038.

*E-mail: ljuzak@brooklyn.cuny.edu. Tel: 718 951 5000, ext. 1426.

Notes

The authors declare no competing financial interest.

ACKNOWLEDGMENTS

This work was sponsored by funding from the National Institutes of Health (NIH 1SC2GM092291 and 5SC3GM105562 to L.J.J.). Time-correlated single photon counting measurements were collected at the Ultrafast Optical Processes Laboratory at the University of Pennsylvania supported by the National Institutes of Health (NIH/NIGMS 9P41GM104605). This research was supported, in part, by a grant of computer time from the City University of New York High Performance Computing Center under NSF Grants CNS-0855217, CNS-0958379, and ACI-1126113. We thank Prof. Terry Dowd for helpful discussion of NMR data.

REFERENCES

- (1) Hutnik, C.; Szabo, A. A Time-Resolved Fluorescence Study of Azurin and Metalloazurin Derivatives. *Biochemistry* **1989**, *28*, 3935–3939.
- (2) Hennecke, J.; Sillen, A.; Huber-Wunderlich, M.; Engelborghs, Y.; Glockshuber, R. Quenching of Tryptophan Fluorescence by the Active-Site Disulfide Bridge in the Dsba Protein from *Escherichia Coli*. *Biochemistry* **1997**, *36*, 6391–6400.
- (3) Teale, F. W. J. Ultraviolet Fluorescence of Proteins in Neutral Solution. *Biochem. J.* **1960**, *76*, 381–388.
- (4) Chen, R. F. Fluorescence Quantum Yields of Tryptophan and Tyrosine. *Anal. Lett.* **1967**, *1*, 35–42.
- (5) Grinvald, A.; Steinberg, I. Z. The Fluorescence Decay of Tryptophan Residues in Native and Denatured Proteins. *Biochim. Biophys. Acta* **1976**, *427*, 663–678.
- (6) Permyakov, E. A.; Burshtein, E. A. Some Aspects of Studies of Thermal Transitions in Proteins by Means of Their Intrinsic Fluorescence. *Biophys. Chem.* **1984**, *19*, 265–271.
- (7) Szabo, A. G.; Faerman, C. Dilemma of Correlating Fluorescence Quantum Yields and Intensity Decay Times in Single Tryptophan Mutant Proteins. *Proc. SPIE-Int. Soc. Opt. Eng.* **1992**, *1640*, 70–80.
- (8) Nanda, V.; Brand, L. Aromatic Interactions in Homeodomains Contribute to the Low Quantum Yield of a Conserved, Buried Tryptophan. *Proteins: Struct., Funct., Genet.* **2000**, *40*, 112–125.
- (9) Verheyden, S.; Sillen, A.; Gils, A.; Declerck, P. J.; Engelborghs, Y. Tryptophan Properties in Fluorescence and Functional Stability of Plasminogen Activator Inhibitor 1. *Biophys. J.* **2003**, *85*, 501–510.
- (10) Callis, P. R.; Liu, T. Quantitative Prediction of Fluorescence Quantum Yields for Tryptophan in Proteins. *J. Phys. Chem. B* **2004**, *108*, 4248–4259.
- (11) Muino, P. L.; Callis, P. R. Solvent Effects on the Fluorescence Quenching of Tryptophan by Amides Via Electron Transfer. Experimental and Computational Studies. *J. Phys. Chem. B* **2009**, *113*, 2572–2577.
- (12) Osysko, A. P.; Muino, P. L. Fluorescence Quenching of Tryptophan and Tryptophanyl Dipeptides in Solution. *J. Biophys. Chem.* **2011**, *2*, 316–321.
- (13) Pan, C.-P.; Muino, P. L.; Barkley, M.; Callis, P. R. Correlation of Tryptophan Fluorescence Spectral Shifts and Lifetimes Arising Directly from Heterogeneous Environment. *J. Phys. Chem. B* **2011**, *115*, 3245–3253.
- (14) McMillan, A. W.; Kier, B. L.; Shu, I.; Byrne, A.; Andersen, N. H.; Parson, W. W. Fluorescence of Tryptophan in Designed Hairpin and Trp-Cage Miniproteins: Measurements of Fluorescence Yields and Calculations by Quantum Mechanical Molecular Dynamics Simulations. *J. Phys. Chem. B* **2013**, *117*, 1790–1809.
- (15) Nakanishi, M.; Tsuboi, M. The Rate of Increase in Fluorescence Intensity Caused by Deuteration of Tryptophan. *Chem. Phys. Lett.* **1978**, *57*, 262–264.
- (16) Shizuka, H.; Serizawa, M.; Kobayashi, H.; Kameta, K.; Sugiyama, H.; Matsuura, T.; Saito, I. Excited-State Behavior of Tryptamine and Related Indoles. Remarkably Efficient Intramolecular Proton-Induced Quenching. *J. Am. Chem. Soc.* **1988**, *110*, 1726–1732.
- (17) Yu, H. T.; Colucci, W. J.; McLaughlin, M. L.; Barkley, M. D. Fluorescence Quenching in Indoles by Excited-State Proton Transfer. *J. Am. Chem. Soc.* **1992**, *114*, 8449–8454.
- (18) Chen, Y.; Barkley, M. D. Toward Understanding Tryptophan Fluorescence in Proteins. *Biochemistry* **1998**, *37*, 9976–9982.
- (19) Eftink, M. R.; Jia, J.; Hu, D.; Ghiron, C. A. Fluorescence Studies with Tryptophan Analogs: Excited State Interactions Involving the Side Chain Amino Group. *J. Phys. Chem.* **1995**, *99*, 5713–5723.
- (20) Chen, Y.; Liu, B.; Yu, H.-T.; Barkley, M. D. The Peptide Bond Quenches Indole Fluorescence. *J. Am. Chem. Soc.* **1996**, *118*, 9271–9278.
- (21) Ababou, A.; Bombarda, E. On the Involvement of Electron Transfer Reactions in the Fluorescence Decay Kinetics Heterogeneity of Proteins. *Protein Sci.* **2001**, *10*, 2102–2113.
- (22) Adams, P. D.; Chen, Y.; Ma, K.; Zagorski, M. G.; Sonnichsen, F. D.; McLaughlin, M. L.; Barkley, M. D. Intramolecular Quenching of Tryptophan Fluorescence by the Peptide Bond in Cyclic Hexapeptides. *J. Am. Chem. Soc.* **2002**, *124*, 9278–9286.
- (23) Hellings, M.; De Maeyer, M.; Verheyden, S.; Hao, Q.; Van Damme, E. J. M.; Peumans, W. J.; Engelborghs, Y. The Dead-End Elimination Method, Tryptophan Rotamers, and Fluorescence Lifetimes. *Biophys. J.* **2003**, *85*, 1894–1902.
- (24) Qiu, W.; Li, T.; Zhang, L.; Yang, Y.; Kao, Y.-T.; Wang, L.; Zhong, D. Ultrafast Quenching of Tryptophan Fluorescence in Proteins: Interresidue and Intrahelical Electron Transfer. *Chem. Phys.* **2008**, *350*, 154–164.
- (25) Cowgill, R. W. Fluorescence and the Structure of Proteins. XVIII. Spatial Requirements for Quenching by Disulphide Bonds. *Biochim. Biophys. Acta* **1970**, *207*, 556–559.
- (26) Eisenberg, A. S.; Juszczak, L. J. Correlation of TrpGly and GlyTrp Rotamer Structure with W7 and W10 UV Resonance Raman Modes and Fluorescence Emission Shifts. *J. Amino Acids* **2012**, *2012*, 10.
- (27) Eisenberg, A. S.; Juszczak, L. J. Relating Trp-Glu Dipeptide Fluorescence to Molecular Conformation: The Role of the Discrete chi 1 and chi 2 Angles. *J. Comput. Chem.* **2013**, *34*, 1549–1560.
- (28) Geuenich, D.; Hess, K.; Köhler, F.; Herges, R. Anisotropy of the Induced Current Density (Acid), a General Method to Quantify and Visualize Electronic Delocalization. *Chem. Rev.* **2005**, *105*, 3758–3772.
- (29) Kim, K. S.; Sung, Y. M.; Matsuo, T.; Hayashi, T.; Kim, D. Investigation of Aromaticity and Photophysical Properties in [18]/[20] Π Porphyrene Derivatives. *Chem. Eur. J.* **2011**, *17*, 7882–7889.
- (30) Berlman, I. B. Empirical Correlation between Nuclear Conformation and Certain Fluorescence and Absorption Characteristics of Aromatic Compounds. *J. Phys. Chem.* **1970**, *74*, 3085–3093.
- (31) Tlach, B. C.; Tomlinson, A. L.; Ryno, A. G.; Knoble, D. D.; Drochner, D. L.; Krager, K. J.; Jeffries-El, M. Influence of Conjugation Axis on the Optical and Electronic Properties of Aryl-Substituted Benzobisoxazoles. *J. Org. Chem.* **2013**, *78*, 6570–6581.
- (32) Niko, Y.; Kawauchi, S.; Otsu, S.; Tokumaru, K.; Konishi, G.-I. Fluorescence Enhancement of Pyrene Chromophores Induced by Alkyl Groups through Σ - Π Conjugation: Systematic Synthesis of Primary, Secondary, and Tertiary Alkylated Pyrenes at the 1, 3, 6, and 8 Positions and Their Photophysical Properties. *J. Org. Chem.* **2013**, *78*, 3196–3207.
- (33) Callis, P. R. Molecular Orbital Theory of the $^1\text{L}_\text{a}$ and $^1\text{L}_\text{b}$ States of Indole. *J. Chem. Phys.* **1991**, *95*, 4230–4240.
- (34) Callis, P. R. In *Methods in Enzymology*; Ludwig Brand, M. L. J., Ed.; Academic Press: Waltham, MA, 1997; Vol. 278, pp 113–150.
- (35) Kirby, E. P.; Steiner, R. F. Influence of Solvent and Temperature Upon the Fluorescence of Indole Derivatives. *J. Phys. Chem.* **1970**, *74*, 4480–4490.
- (36) White, A. Effect of pH on Fluorescence of Tyrosine, Tryptophan and Related Compounds. *Biochem. J.* **1959**, *71*, 217–220.
- (37) Hür, D.; Güven, A. The Acidities of Some Indoles. *J. Mol. Struct.: THEOCHEM* **2002**, *583*, 1–18.

- (38) Somers, K. R. F.; Kryachko, E. S.; Ceulemans, A. Theoretical Study of Indole: Protonation, Indolyl Radical, Tautomers of Indole, and Its Interaction with Water. *Chem. Phys.* **2004**, *301*, 61–79.
- (39) Li, J.-N.; Liu, L.; Fu, Y.; Guo, Q.-X. What Are the Pka Values of Organophosphorus Compounds? *Tetrahedron* **2006**, *62*, 4453–4462.
- (40) Sobolewski, A.; Domcke, W. *Ab Initio* Investigations on the Photophysics of Indole. *Chem. Phys. Lett.* **1999**, *315*, 293–298.
- (41) Dowd, T. *Personal communication*, October 21, 2013.
- (42) Krygowski, T. M. Crystallographic Studies of Inter- and Intramolecular Interactions Reflected in Aromatic Character Of π -Electron Systems. *J. Chem. Inf. Comput. Sci.* **1993**, *33*, 70–78.
- (43) Schleyer, P. v. R.; Maerker, C.; Dransfeld, A.; Jiao, H.; Hommes, N. J. R. v. E. Nucleus-Independent Chemical Shifts: A Simple and Efficient Aromaticity Probe. *J. Am. Chem. Soc.* **1996**, *118*, 6317–6318.
- (44) Randic, M. Aromaticity and Conjugation. *J. Am. Chem. Soc.* **1977**, *99*, 444–450.
- (45) Slater, L. S.; Callis, P. R. Molecular Orbital Theory of the $^1\text{L}_a$ and $^1\text{L}_b$ States of Indole. 2. An *Ab Initio* Study. *J. Phys. Chem.* **1995**, *99*, 8572–8581.
- (46) Lackowicz, J. *Principles of Fluorescence Spectroscopy*, 3rd ed.; Springer Science + Business Media LLC: New York, 2006.
- (47) Callis, P. R. In *Reviews in Fluorescence*; Geddes, C., Ed.; Springer: New York, 2007; Vol. 4, pp 199–248.
- (48) Callis, P. R.; Vivian, J. T. Understanding the Variable Fluorescence Quantum Yield of Tryptophan in Proteins Using QM-MM Simulations. Quenching by Charge Transfer to the Peptide Backbone. *Chem. Phys. Lett.* **2003**, *369*, 409–414.
- (49) Callis, P. R.; Petrenko, A.; Muino, P. L.; Tusell, J. R. *Ab Initio* Prediction of Tryptophan Fluorescence Quenching by Protein Electric Field Enabled Electron Transfer. *J. Phys. Chem. B* **2007**, *111*, 10335–10339.
- (50) Shemesh, D.; Sobolewski, A. L.; Domcke, W. Role of Excited-State Hydrogen Detachment and Hydrogen-Transfer Processes for the Excited-State Deactivation of an Aromatic Dipeptide: N-Acetyl Tryptophan Methyl Amide. *Phys. Chem. Chem. Phys.* **2010**, *12*, 4899–4905.
- (51) Dian, B. C.; Longarte, A.; Zwier, T. S. Hydride Stretch Infrared Spectra in the Excited Electronic States of Indole and Its Derivatives: Direct Evidence for the $^1\pi \sigma^*$ State. *J. Chem. Phys.* **2003**, *118*, 2696–2706.
- (52) Van Gilst, M.; Hudson, B. S. Histidine-Tryptophan Interactions in T4 Lysozyme: ‘Anomalous’ pH Dependence of Fluorescence. *Biophys. Chem.* **1996**, *63*, 17–25.
- (53) Shinitzky, M.; Goldman, R. Fluorometric Detection of Histidine-Tryptophan Complexes in Peptides and Proteins. *Eur. J. Biochem.* **1967**, *3*, 139–144.
- (54) Loewenthal, R.; Sancho, J.; Fersht, A. R. Fluorescence Spectrum of Barnase: Contributions of Three Tryptophan Residues and a Histidine-Related pH Dependence. *Biochemistry* **1991**, *30*, 6775–6779.
- (55) De Beuckeleer, K.; Volckaert, G.; Engelborghs, Y. Time Resolved Fluorescence and Phosphorescence Properties of the Individual Tryptophan Residues of Barnase: Evidence for Protein-Protein Interactions. *Proteins: Struct., Funct., Bioinf.* **1999**, *36*, 42–53.
- (56) Weaver, L. H.; Matthews, B. W. Structure of Bacteriophage T4 Lysozyme Refined at 1.7 Å Resolution. *J. Mol. Biol.* **1987**, *193*, 189–199.
- (57) Sánchez, M.; Jennings, P. A.; Murre, C. Conformational Changes Induced in HOXb-8/PBX-1 Heterodimers in Solution and Upon Interaction with Specific DNA. *Mol. Cell. Biol.* **1997**, *17*, 5369–5376.
- (58) Sprules, T.; Green, N.; Featherstone, M.; Gehring, K. Lock and Key Binding of the HOX YPWM Peptide to the PBX Homeodomain. *J. Biol. Chem.* **2003**, *278*, 1053–1058.
- (59) Rusakowicz, R.; Testa, A. C. 2-Aminopyridine as a Standard for Low-Wavelength Spectrofluorimetry. *J. Phys. Chem.* **1968**, *72*, 2680–2681.
- (60) DAS 6 User’s Guide, version E, part no. J81119. Horiba, Inc.: Edison, NJ, 2012.
- (61) Weast, R. *Handbook of Chemistry and Physics*, 53 ed.; Chemical Rubber Company Press: Boca Raton, FL, 1972.
- (62) Goldberg, J. M.; Speight, L. C.; Fegley, M. W.; Petersson, E. J. Minimalist Probes for Studying Protein Dynamics: Thioamide Quenching of Selectively Excitable Fluorescent Amino Acids. *J. Am. Chem. Soc.* **2012**, *134*, 6088–6091.
- (63) Frisch, M. J.; Trucks, G. W.; Schlegel, H. B.; Scuseria, G. E.; Robb, M. A.; Cheeseman, J. R.; Scalmani, G.; Barone, V.; Mennucci, B.; Petersson, G. A.; et al. *Gaussian 09*, revision A.02. Gaussian, Inc.: Wallingford, CT, 2009.
- (64) Varetto, U. *MOLEKEL*, version 5.4.0.8; Swiss National Supercomputing Centre: Lugano, Switzerland, 2009.
- (65) Laaksonen, L. L. *p gOpenMol*, 1.31 ed.; Center of Scientific Computations: Espoo, FI, 1999.
- (66) Hess, B.; Kutzner, C.; van der Spoel, D.; Lindahl, E. Gromacs 4: Algorithms for Highly Efficient, Load-Balanced, and Scalable Molecular Simulation. *J. Chem. Theory Comput.* **2008**, *4*, 435–447.